

Electron capture in collisions of S with H⁺

L. B. Zhao* and P. C. Stancil[†]

Department of Physics and Astronomy and the Center for Simulational Physics

The University of Georgia, Athens, GA, 30602-2451

J.-P. Gu, H.-P. Liebermann, P. Funke, and R. J. Buenker[‡]

Fachbereich C-Mathematik und Naturwissenschaften,

Bergische Universität Wuppertal, D-42097 Wuppertal, Germany

M. Kimura[§]

Graduate School of Sciences, Kyushu University, Fukuoka 812-8581, Japan

(Dated: January 22, 2005)

Abstract

Within the framework of a fully quantum mechanical molecular-orbital close-coupling (QMOCC) theory, charge transfer has been studied for collisions of S with H⁺. The multireference single- and double-excitation configuration-interaction (MRD-CI) method was utilized to evaluate the adiabatic potentials and nonadiabatic coupling matrix elements for the SH⁺ system. Cross sections and rate coefficients are presented for S(³P, ¹D) + H⁺ → S⁺(⁴S^o, ²D^o, ²P^o) + H with relative collision energies between 0.1 meV/u and 10 keV/u and temperatures between 10 K and 2.0 × 10⁶ K. The investigation shows that the charge-transfer process is dominated by S(³P) + H⁺ → S⁺(²P^o) + H and that the cross sections and rate coefficients vary by orders of magnitude over the energy and temperature range considered. The current rate coefficients are in disagreement with the often adopted value of 1.30 × 10⁻⁹ cm³/s at low temperatures, and two orders of magnitude smaller than a previous estimate at T = 10⁴ K, for the process S(³P) + H⁺ → S⁺(²D^o, ²P^o) + H. The QMOCC cross sections are compared with those from a semiclassical molecular-orbital close-coupling method and application of the results to astrophysical environments is briefly discussed.

PACS numbers: 34.10.+x, 34.20.Mq, 34.70.+e

*Electronic address: zhao@physast.uga.edu

[†]Electronic address: stancil@physast.uga.edu

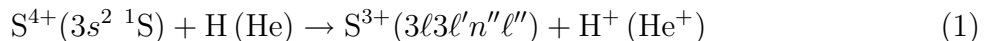
‡Electronic address: buenker@uni-wuppertal.de

§Electronic address: mineoscc@mbox.nc.kyushu-u.ac.jp

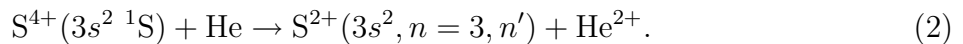
I. INTRODUCTION

Intense efforts have lasted for many years towards understanding charge-transfer processes in ion-atom collisions because of its fundamental physical interest [1] and application importance in investigations of controlled fusion plasmas, planetary atmospheres, and astrophysical environments [2, 3]. For instance, in a fusion reactor, ions can interact with neutral atoms injected into the reactor from the reactor wall or pumped into the reactor and charge transfer may occur in such collisions. As a consequence, excited states of ions produced by charge transfer can be populated and subsequently decay through radiative emission. By measuring the intensity of the emitted lines, properties of the plasma, such as temperature, electron density, and charge states, can be determined [4, 5]. The line emission produced in charge-transfer reactions is also utilized to diagnose the composition and properties of terrestrial and non-terrestrial plasmas, such as comets [6], planetary nebulae, and supernova remnants [7, 8]. In particular, Baliunas and Butler [9] found that charge transfer plays an important role as an ionization source in many astrophysical plasmas. Consequently, theoretical and experimental studies on charge transfer for a variety of ion-atom systems have been published (see e.g. [10–13] and references therein).

However, less attention has been paid to sulfur systems. Recently, Stancil and coworkers [14, 15] reported on electron capture following S^{4+} collisions with hydrogen and helium



and



Several different theoretical approaches, including the quantum mechanical molecular-orbital close-coupling, atomic-orbital close-coupling, classical trajectory Monte Carlo, and continuum distorted wave methods were adopted in their calculations. The work was mainly motivated by observations of X-rays from solar system objects (e.g. [16, 17]). Investigations into planetary and other gaseous nebulae also appeal to the charge-transfer mechanism. Péquignot, Aldrovandi, and Stasinska [18] showed that the intensities of the line spectrum for neutral sulfur in models of the planetary nebula NGC 7027 were underestimated and hence it was proposed to include charge-transfer processes in the simulation of these lines. Furthermore, the standard static photoionization model met difficulties in attempting to ac-

count for the ionization structure of NGC 7027. The main discrepancies can be eliminated when including the charge-transfer reactions for $S^{q+} + H$ and other systems. However, for $S(^3P) + H^+$ and $S^+ + H$, they adopted rate coefficients of 1.0×10^{-9} and $3.0 \times 10^{-8} \times \exp(-37800/T)$ cm^3/s for the exo- and endothermic reactions, respectively, which were merely speculation. In order to model gaseous nebulae including sulfur ions and atoms, it is essential to provide reliable charge-transfer rate coefficients for these systems.

To the best of our knowledge, no experiment has been performed on charge transfer for collisions of S with H^+ . The only theoretical study was made within a semiclassical framework [19], in which the relative motion of nuclei is described classically, while electronic motions are treated quantum mechanically. In the work of Kimura *et al.* [19], relative collision energies considered for S with H^+ were from a few eV to ~ 20 keV. In the present paper, we report on a fully quantum mechanical calculation for the same system,



The multireference single- and double-excitation configuration-interaction method (MRD-CI) [20] is utilized to evaluate the molecular electronic structure of SH^+ and the relative motion of the nuclei is characterized with the quantum-mechanical molecular-orbital close-coupling (QMOCC) approach [21]. The collision energies in the present QMOCC calculation are between 0.1 meV/u and 10 keV/u.

In Sec. II, the calculations of the molecular potentials and nonadiabatic radial and rotational coupling matrices are described for the SH^+ system. In Sec. III, the QMOCC theory is briefly outlined. In Sec. IV, total and state-selective cross sections and rate coefficients are presented and compared to those from the semiclassical molecular-orbital close-coupling (SCMOCC) method. Sec. V summarizes the main results.

II. MOLECULAR ELECTRONIC STRUCTURE CALCULATIONS

The multireference single- and double-excitation configuration-interaction method employed in this paper has been detailed earlier by Buenker and coworkers [20, 22]. Here only information relevant to the present calculation is specified. Further details can be found in Refs. [19, 20, 22]. The atomic orbital basis sets for the molecular calculations consist of contracted Gaussian functions. For the sulfur atom, the $(12s9p)$ basis was contracted

into $[6s5p]$ and augmented with two d and f polarization functions. The exponents for s -, p - and d -type Rydberg functions have been reoptimized to give 0.023, 0.020, and 0.015, respectively. The final contracted basis set was taken to be $[7s6p3d1f]$. For the hydrogen atom, the $(7s3p)$ basis was contracted into $[5s3p]$ and one six-component d -type Rydberg function with a reoptimized exponent of 1.0 was added.

The adiabatic potentials for all molecular electronic states corresponding to the asymptotic limits $S(3p^4\ ^3P, ^1D, ^1S) + H^+$ and $S^+(3p^3\ ^4S^o, ^2D^o, ^2P^o) + H$ and nonadiabatic radial and rotational coupling matrix elements between these states have been obtained from internuclear distance $R = 2$ to 12 a.u. The two electronic states $1\ ^3\Sigma^-$ and $1\ ^5\Sigma^-$ are formed in the approach of $S^+(3p^3\ ^4S^o)$ with H, the six states $1\ ^1\Sigma^-$, $2\ ^3\Sigma^-$, $1\ ^1\Pi$, $1\ ^3\Pi$, $1\ ^1\Delta$, and $1\ ^3\Delta$ by $S^+(3p^3\ ^2D^o)$ with H, the four states $1\ ^1\Sigma^+$, $2\ ^3\Sigma^+$, $2\ ^1\Pi$, and $2\ ^3\Pi$ by $S^+(3p^3\ ^2P^o)$ with H, the two states $3\ ^3\Sigma^-$ and $3\ ^3\Pi$ by $S(3p^4\ ^3P)$ with H^+ , the three states $2\ ^1\Sigma^+$, $3\ ^1\Pi$ and $2\ ^1\Delta$ by $S(3p^4\ ^1D)$ with H^+ , and the state $3\ ^1\Sigma^+$ by $S(3p^4\ ^1S)$ with H^+ . The calculated MRD-CI asymptotic energies are presented for the eighteen molecular states relative to the $S(3p^4\ ^3P) + H^+$ channel and compared with experimental energies [23] in Table I. The maximum absolute error of the current results from the experimental data is 0.264 eV. In Fig. 1 (a) and (b), the adiabatic potential energies (solid curves) are plotted as a function of internuclear distance R for the eight triplet and eight singlet molecular states. We do not consider charge transfer from $3\ ^1\Sigma^+$ into any possible final states, and from any possible initial states into $1\ ^5\Sigma^-$ due to their small contributions. Thus only transitions from the triplet states $3\ ^3\Sigma^-$ and $3\ ^3\Pi$ into $1\ ^3\Sigma^-$, $1\ ^3\Pi$, $2\ ^3\Sigma^-$, $1\ ^3\Delta$, $2\ ^3\Pi$, and $1\ ^3\Sigma^+$, and from the singlet states $2\ ^1\Sigma^+$, $3\ ^1\Pi$, and $2\ ^1\Delta$ into $1\ ^1\Pi$, $1\ ^1\Delta$, $1\ ^1\Sigma^-$, $2\ ^1\Pi$, and $1\ ^1\Sigma^+$ are included in the current calculations.

In Figs. 2 and 3, all the nonadiabatic radial couplings and representative rotational couplings are plotted as a function of R . Figs. 2 (a) and 3 (a) display the couplings among the triplet states, while 2 (b) and 3 (b) give the couplings among the singlet states. The potentials have been transformed from the adiabatic representation to the diabatic representation using Eqs. (8-10) (see Sec. III for details). The diagonal diabatic potential energies (dashed curves) are displayed in Fig. 1 and the representative off-diagonal matrix elements plotted in Fig. 4.

Beyond $R = 12.0$ a.u., the potentials are described by the charge-quadrupole and charge-

induced-dipole interactions

$$V_L(R) = -\frac{\alpha_d}{2R^4} + \xi_\Lambda \frac{\langle r^2 \rangle}{R^3} + E_\infty, \quad (4)$$

where α_d is the dipole polarizability of the neutral atoms, ξ_Λ with $\Lambda = 0, 1, 2, \dots$ is an angular parameter, $\langle r^2 \rangle$ is the mean square radius, and E_∞ is the separated-atom energy. All the quantities in Eq. (4) are in atomic units. α_d for sulfur atoms in the ground and excited states are taken from Ref. [24], and ξ_Λ and $\langle r^2 \rangle$ are from Refs. [25] and [26], respectively. Table II lists these parameters. E_∞ is determined using these parameters and the *ab initio* potentials.

III. CLOSE-COUPPLING THEORY

A quantum-mechanical molecular-orbital close-coupling (QMOCC) approach to describe electron capture in ion-atom collisions has been formulated by Zygelman *et al.* [21]. Here we only briefly outline the main theoretical aspects and formulae.

The scattering wave function for ion-atom systems may be written in the form

$$\Psi(\mathbf{r}, \mathbf{R}) = \sum_{\gamma} \psi_{\gamma}(\mathbf{r}, \mathbf{R}) F_{\gamma}(\mathbf{R}), \quad (5)$$

where $\psi_{\gamma}(\mathbf{r}, \mathbf{R})$ is the adiabatic electronic eigenfunctions, $\mathbf{r} = \{\mathbf{r}_1, \mathbf{r}_2, \mathbf{r}_3 \dots\}$ and \mathbf{R} denote coordinates of all molecular electrons and the relative nuclear motion, respectively, and $F_{\gamma}(\mathbf{R})$ is the effective scattering amplitude for the γ th-channel. In principle, the summation of Eq. (5) is infinite, but it is truncated in practical calculations to make the resulting coupled equations tractable; namely the so-called close-coupling approximation is adopted.

Substituting Eq. (5) into the Schrödinger equation for the ion-atom system and following the procedure of Zygelman *et al.* [21], the resulting set of coupled equations is given by

$$-\frac{1}{2\mu} [\underline{I}\nabla_{\mathbf{R}} - i\underline{A}(\mathbf{R})]^2 \underline{F}(\mathbf{R}) + \underline{V}(R)\underline{F}(\mathbf{R}) = E\underline{F}(\mathbf{R}), \quad (6)$$

where μ is the nuclear reduced mass of the ion-atom pair, E is the relative collision energy in the center-of-mass frame, \underline{I} denotes a unit matrix, $\underline{V}(R)$ is a diagonal matrix with elements consisting of adiabatic eigenvalues for each channel state with $|\mathbf{R}| = R$, and $\underline{A}(\mathbf{R})$ is the vector potential of the form $[\underline{A}(\mathbf{R})]_{\alpha\beta} = i\langle \psi_{\alpha} | \nabla_{\mathbf{R}} | \psi_{\beta} \rangle$. Here we emphasize that the same notation has been employed as in Ref. [21] and the underlined quantities represent matrices.

In the adiabatic representation, transitions from a molecular state to another molecular state are driven by the vector potential $\underline{A}(\mathbf{R})$ including both the radial $\underline{A}^{rad}(R)$ and rotational $\underline{A}^{rot}(R)$ components. However, it is numerically more convenient to perform the scattering calculations in a diabatic representation which can be obtained with a unitary transformation. By making such a transformation to Eq. (6), the set of the coupled equations in the diabatic representation is given by

$$-\frac{1}{2\mu}I\nabla_{\mathbf{R}}^2\underline{G}(\mathbf{R}) + \underline{U}(R)\underline{G}(\mathbf{R}) = E\underline{G}(\mathbf{R}), \quad (7)$$

where $\underline{G}(\mathbf{R}) = \underline{W}(R)\underline{F}(\mathbf{R})$ and $\underline{U}(R)$ is the diabatic potential matrix whose off-diagonal elements are responsible for driving charge transfer in the diabatic representation, defined by

$$\underline{U}(R) = \underline{W}(R)[\underline{V}(R) - \underline{P}(R)]\underline{W}^{-1}(R). \quad (8)$$

$\underline{W}(R)$ is the unitary matrix that obeys the equation

$$\frac{d\underline{W}(R)}{dR} + i\underline{W}(R)\underline{A}^{rad}(R) = 0, \quad (9)$$

and $\underline{P}(R)$ is a coupling matrix whose elements are given by [13, 27]

$$P_{\alpha\beta} = \mp \frac{1}{\mu R^2} [(J \mp \Lambda_\alpha)(J \pm \Lambda_\alpha + 1)]^{1/2} A_{\alpha\beta}^{rot} \delta(\Lambda_\alpha, \Lambda_\beta \mp 1), \quad (10)$$

where J is the total angular momentum, and Λ is the component of electronic angular momenta along the internuclear axis. It should be stressed that Eq. (9) differs from the corresponding equation in Ref. [21], where a typographical error was corrected by Zygelman *et al.* [28].

By introducing a partial-wave decomposition for $\underline{G}(\mathbf{R})$, Eq. (7) can be further simplified. The resulting set of radial coupled equations may be solved with the log-derivative method of Johnson [29]. From the numerical results of the log-derivative and the asymptotic expressions of the radial functions, the \underline{K} matrix may be extracted and thus the scattering matrix \underline{S} is obtained

$$\underline{S}_J = \frac{\underline{I} + i\underline{K}_J}{\underline{I} - i\underline{K}_J}. \quad (11)$$

Finally the charge transfer cross sections from channel α to channel β is expressed in terms of the scattering matrix elements

$$\sigma_{\alpha \rightarrow \beta} = \frac{\pi g_\alpha}{k_\alpha^2} \sum_J (2J + 1) |\underline{S}_J|_{\alpha\beta}^2, \quad (12)$$

where k_α denotes the wave number for center-of-mass motion of the initial ion-atom channel, and g_α is an approach probability factor of the initial channel α . Electron translation factors (ETFs; e.g. [30]) are not included in the current calculations, since the influence of ETFs is expected to be important for $E > 1$ keV/u (e.g. [31, 32]). Our results may be uncertain above this energy, but probably by no more than 50%.

IV. RESULTS AND DISCUSSION

State-to-state cross sections for charge-transfer processes $3\ ^3\Sigma^-, 3\ ^3\Pi \rightarrow 1\ ^3\Sigma^-, 1\ ^3\Pi, 2\ ^3\Sigma^-, 1\ ^3\Delta, 2\ ^3\Pi$, and $1\ ^3\Sigma^+$, and $2\ ^1\Sigma^+, 3\ ^1\Pi, 2\ ^1\Delta \rightarrow 1\ ^1\Pi, 1\ ^1\Delta, 1\ ^1\Sigma^-, 2\ ^1\Pi$, and $1\ ^1\Sigma^+$ are evaluated by using the molecular electronic structure and coupling data in Sec. II. The contributions from the individual partial waves are summed as in Eq. (12) until a convergence of the cross sections is achieved. The results are illustrated as a functions of relative collision energy in Fig. 5. The energy ranges from 0.1 meV/u to 10 keV/u. (a) and (b) represent electron capture into the molecular states $1\ ^3\Sigma^-, 1\ ^3\Pi, 2\ ^3\Sigma^-, 1\ ^3\Delta, 2\ ^3\Pi$, and $1\ ^3\Sigma^+$ from $3\ ^3\Sigma^-$ and $3\ ^3\Pi$, while (c), (d), and (e) correspond to capture into the molecular states $1\ ^1\Pi, 1\ ^1\Delta, 1\ ^1\Sigma^-, 2\ ^1\Pi$, and $1\ ^1\Sigma^+$ from the $2\ ^1\Sigma^+, 3\ ^1\Pi$, and $2\ ^1\Delta$ states. The cross sections for the different transitions vary in magnitude over a wide range. The cross sections in Fig. 5 (a) show drops at ~ 4 meV/u for all transitions. These drops are due to a potential barrier in the initial $3\ ^3\Pi$ state as a consequence of the quadrupole term in the long-range expansion given in Eq. (4). The barrier has a height of ~ 3.7 meV at $R = 12.35$ a.u. Similarly drops occur at ~ 10 meV/u in Fig. 5 (c) and (d). The drops in Fig. 5 (d) are ascribed to a potential barrier of height of 8.5 meV at $R = 9.4$ a.u. in the initial $3\ ^1\Pi$ state. However, at ~ 10 meV in the $2\ ^1\Sigma^+$ state, there exists no potential barrier which may give rise to the drops in Fig. 5 (c). The drops in Fig. 5 (c) may be also caused by the barrier in the $3\ ^1\Pi$ state. The barrier acts on electron capture from the initial $2\ ^1\Sigma^+$ state with the help of the rotational coupling between the $2\ ^1\Sigma^+$ and $3\ ^1\Pi$ states. We have confirmed this assumption by removing this coupling in the calculation; namely the drops in Fig. 5 (c) disappear if the rotational coupling is not included.

Different from all the transitions in Fig. 5. (a), (c) and (d), the curves in Fig. 5 (b) and (e) do not display sudden drops in the low energy region. On the contrary, the background cross sections, excluding resonances, increase monotonically as the relative collision energy

decreases from a few meV/u to 0.1 meV/u. This is because the initial molecular states, $3\ ^3\Sigma^-$ and $2\ ^1\Delta$, are purely attractive at long-range, rather than possessing a potential barrier. For most of the transitions illustrated in Fig. 5, rich resonance structures may be seen in the low energy region between 0.1 meV/u to 10 meV/u. All these resonances are interpreted in terms of quasibound states associated with classical orbiting. For example, the resonances at 0.4 and 1.0 meV/u in Fig. 5 (a) and at 0.84 meV/u in Fig. 5 (b) are due to the presence of the quasibound states in the initial states $3\ ^3\Pi$ and $3\ ^3\Sigma^-$, respectively. Seemingly, no resonance appears in the $3\ ^3\Pi \rightarrow 2\ ^3\Pi$ transition. However, a fine-energy-grid analysis found that the exact resonance positions are at 0.407 and 0.995 meV/u. Similar phenomena have been found in the charge-transfer reactions $N^{3+} + H \rightarrow N^{2+} + H^+$ [33] and $N^{5+} + H \rightarrow N^{4+} + H^+$ [34]. Both the charge-transfer cross sections for $N^{3+} + H$ calculated by Ritty *et al.* [33] and those for $N^{5+} + H$ by Shimakura and Kimura [34] displayed rich resonance structures in the low energy region. Close to 1 eV/u, the cross sections for all the transitions in Fig. 5 start to increase with increasing E . This is because the possibility for the system to penetrate the inner region (small and intermediate R) becomes larger with increasing E , while stronger couplings between the molecular states occur for $R < 7.0$ a.u. as seen in Fig. 4.

In Fig. 6, the partial electron capture cross sections are illustrated and compared with the SCMOCC results of Ref. [19]. (a) represents electron capture into the $S^+(^4S^o, ^2D^o, ^2P^o) + H$ channels owing to $S(^3P) + H^+$ collisions, while (b) corresponds to capture into the $S^+(^2D^o, ^2P^o) + H$ channels owing to $S(^1D) + H^+$ collisions. Our QMOCC calculations show that the charge-transfer process $S(^3P) + H^+ \rightarrow S^+(^2P^o) + H$ dominates in the entire energy range considered. From 0.1 meV/u to 1 eV/u, the QMOCC cross sections for capture into $S^+(^2P^o)$ are approximately two orders of magnitude larger than those for capture into $S^+(^2D^o)$ for collisions of $S(^3P)$ with H^+ , and the cross sections for capture into $S^+(^4S^o)$ is even smaller. For $S(^1D) + H^+$ collisions, below 0.4 eV/u, the cross sections for capture into $S^+(^2D^o)$ are much larger than those for capture into $S^+(^2P^o)$, while from 0.4 eV/u to 10 keV/u, the cross sections into the two states are comparable. $S(^1D) + H^+$ collisions do not contribute to capture into $S^+(^4S^o)$ because the process is spin-forbidden.

In general, the SCMOCC method gives cross sections in good agreement with those obtained from the QMOCC approach except for low energies. However, the current QMOCC cross sections differ significantly from the SCMOCC results given by Kimura *et al.* [19], as

displayed from 1 eV/u to 10 keV/u in Fig. 6. The discrepancies, varying from a factor of a few to more than one order of magnitude, may stem partly from the increase in the number of channels. Kimura *et al.* included only five channels, while three more channels, $1\ ^3\Sigma^-$, $1\ ^3\Delta$ and $1\ ^3\Sigma^+$, for $S(^3P) + H^+$ collisions and $1\ ^1\Delta$, $1\ ^1\Sigma^-$ and $2\ ^1\Delta$ for $S(^1D) + H^+$ collisions, have been added in the current work. In addition, the semiclassical cross sections of Kimura *et al.* for capture into the $S^+(^2P^o)$ and $S^+(^2D^o)$ states suggested slight out-of-phase oscillatory behaviour, which are not evident in the QMOCC calculations, at intermediate energies. This indicates that there does not exist an obvious interference between the initial and final channels. It should be pointed out that we also made calculations which included the same channels considered by Kimura *et al.* and found the discrepancies to persist, although reduced. Our five-channel results also show that the capture cross sections from the excited state $S(^1D)$ are smaller than those from the ground state. This point is in agreement with Kimura *et al.*'s conclusion.

Rate coefficients are evaluated by averaging the QMOCC cross sections in Fig. 6 (a) and (b) over a Maxwellian velocity distribution. The resulting rate coefficients are plotted as a function of temperature T in Fig. 7 and tabulated in Table III. Figure 7 (a) and (b) correspond to electron capture for $S(^3P) + H^+$ and $S(^1D) + H^+$ collisions, respectively. Figure 7 (a) illustrates that the total electron capture rate coefficients from the ground state $S(^3P)$ for temperatures between 10 K and 2.0×10^6 K are dominated by capture into the $S^+(^2P^o) + H$ channel. The contributions to the total rate coefficients from capture into $S^+(^4S^o)$ and $S^+(^2D^o)$ are negligible below 10^4 K, but the contributions increase with increasing T approaching 27% of the total rate coefficient at 2.0×10^6 K. In the temperature region considered, our QMOCC rate coefficients vary in magnitude over a wide range. For example, for the process $S(^3P) + H^+ \rightarrow S^+(^2P^o) + H$, the rate coefficient is 3.16×10^{-13} cm³/s at $T = 20$ K, it increases monotonically with increasing T , reaching 3.20×10^{-8} cm³/s at $T = 2 \times 10^6$ K. From Fig. 7 (a), the QMOCC total rate coefficient at 10^4 K is two orders of magnitude smaller than an estimation by Butler and Dalgarno [35]. The charge-transfer rate coefficient for $S(^3P) + H^+$ was suggested to be 1.30×10^{-9} cm³/s in the UMIST database for astrochemistry 1999 [36]. This value was thought to be valid for a wide temperature range from 10 to 41000 K. Kingdon and Ferland [37], in a compilation of charge-transfer rate coefficients for the photoionization spectra modeling code Cloudy, assumed that the process was dominated by radiative charge transfer and therefore adopted

a constant rate coefficient of 10^{-14} cm³/s for temperatures between 1000 and 10^4 K. However, our calculations do not support either value. From Fig. 7 (b), below about 2000 K, the total S(¹D) rate coefficients are dominated by capture into the S⁺(²D^o) + H channel, but above about 2000 K, the rate coefficients for processes for capture to S⁺(²D^o) + H and → S⁺(²P^o) + H are comparable. Furthermore, the rate coefficients from the ground state S(³P) are much larger than those from the excited state S(¹D) for the entire temperatures range considered. The differences vary from a factor of a few to several orders of magnitude.

V. ASTROPHYSICAL APPLICATIONS

A potentially important application of the current charge-transfer calculations is to studies of young stellar objects (YSOs). Shang *et al.* [38] have developed a thermal-chemical model to describe the accretion disks of YSOs and to predict the strengths of forbidden emission lines. In particular, they considered the ²D_{3/2} → ⁴S (6731 Å) and ²D_{5/2} → ⁴S (6716 Å) transitions of S II and the 6300 Å line of O I. The 6717/6731 and 6731/6300 line ratios are diagnostics of electron density and temperature, respectively. While they included in their model the charge exchange of O⁺ with H and its reverse to determine the oxygen ionization fraction, they assumed that all sulfur was singly ionized. Table III shows that S⁺ is created from collisions of S(³P) with H⁺ with a rate coefficient at 10^4 K of 1.8×10^{-11} cm³s⁻¹. On the other hand, Butler and Dalgarno [35] have estimated a rate coefficient for the reverse process S⁺ + H, which is endoergic, of 3×10^{-15} cm³/s. While this value could be improved and it is likely that most of the sulfur in YSOs will be singly ionized, as assumed by Shang *et al.* [38], an explicit calculation of the sulfur ionization fraction is desirable.

VI. SUMMARY

Using the quantum-mechanical molecular-orbital close-coupling approach, charge transfer has been investigated for collisions of S and H⁺. We adopted the multireference single- and double-excitation configuration-interaction (MRD-CI) method to evaluate the molecular electronic structure and coupling matrix elements between the adiabatic molecular states for the SH⁺ system. Cross sections are presented for electron capture into the S⁺(⁴S^o, ²D^o, ²P^o) + H channels for collisions of S(³P, ¹D) with H⁺ with relative collision energies between

0.1 meV/u and 10 keV/u. Rate coefficients are given for temperatures between 10 K and 2.0×10^6 K. Our calculations show that the charge-transfer process is dominated by the $S(^3P) + H^+ \rightarrow S^+(^2P^o) + H$ reaction and electron capture from the excited-state channel $S(^1D) + H^+$ is smaller. In the low energy region, a rich resonance structure is found. The resonances are interpreted in terms of quasibound states associated with classical orbiting. Furthermore, the charge-transfer cross sections and rate coefficients vary in magnitude over a wide energy and temperature range. The rate coefficients are in pronounced disagreement with the values adopted in the recent UMIST database for astrochemistry and in the spectral modeling package Cloudy. Furthermore, our QMOCC total rate coefficient is found to be 1.75×10^{-11} cm³/s at $T = 10^4$ K for the process $S(^3P) + H^+$. The value is two orders of magnitude smaller than an estimation by Butler and Dalgarno [35]. The QMOCC cross sections have been compared with those from a semiclassical molecular-orbital close-coupling method. The discrepancies vary roughly from a factor of a few to more than one order of magnitude. Experimental studies for this system may be interesting to test the present theoretical results.

Acknowledgments

LBZ and PCS acknowledge support from NASA grant NAG5-11453 and NSF grant INT-0300708; RJB, JPG and PF acknowledge financial support from the Deutsche Forschungsgemeinschaft grant Bu 450/7-3 and the Fonds der Chemischen Industrie; and MK acknowledges support from the Ministry of Education, Science, Sport, Culture and Technology, Japan Society for Promotion of Science (JSPS) for the US-JP Collaborative Research Program, and Collaborative Research Grant by National Institute for Fusion Science.

-
- [1] J. A. Tanis, A. L. Landers, D. J. Pole, A. S. Alnaser, S. Hossain, and T. Kirchner, *Phys. Rev. Lett.* **92**, 133201 (2004).
 - [2] R. K. Janev, *Review of Fundamental Processes and Applications of Atoms and Ions* (World Scientific, Singapore, 1993).
 - [3] G. J. Ferland, *Annu. Rev. Astron. Astrophys.* **41**, 517 (2003).

- [4] M. G. von Hellermann, W. G. F. Core, J. Frieling, L. D. Horton, R. W. T. Konig, W. Mandl, and H. P. Summers, *Plasma Phys. Control Fusion* **35**, 799 (1993).
- [5] E. J. Synakowski, R. E. Bell, R. V. Budny, C. E. Bush, P. C. Efthimion, B. Grek, D. W. Johnson, L. C. Johnson, B. LeBlanc, H. Park, A. T. Ramsey, and G. Taylor, *Phys. Rev. Lett.* **75**, 3689 (1995).
- [6] C. M. Lisse, D. J. Christian, K. Dennerl, K. J. Meech, R. Petre, H. A. Weaver, and S. J. Wolk, *Science* **292** 1343, (2001).
- [7] F. P. Keenan, C. A. Ramsbottom, K. L. Bell, K. A. Berrington, A. Hibbert, W. A. Feibelman, and W. P. Blair, *Astrophys. J.* **438**, 500 (1995).
- [8] A. D. Silber, S. F. Anderson, B. Margon, and R. A. Downers, *Astrophys. J.* **462**, 428 (1996).
- [9] S. L. Baliunas and S. E. Butler, *Astrophys. J. Lett.* **235**, L45 (1980).
- [10] M. Gargaud, R. McCarroll, and P. Valiron, *Astron. Astrophys.* **106**, 197 (1983).
- [11] E. Wolfrum, J. Schweinzer, and H. Winter, *Phys. Rev. A* **45**, R4218 (1992).
- [12] P. C. Stancil, J.-P. Gu, C. C. Havener, P. S. Krstić, D. R. Schultz, M. Kimura, B. Zygelman, G. Hirsch, R. J. Buenker and M. E. Bannister, *J. Phys. B* **31**, 3647 (1998).
- [13] A. R. Turner, D. L. Cooper, J. G. Wang, and P. C. Stancil, *Phys. Rev. A* **68**, 012704 (2003).
- [14] P. C. Stancil, A. R. Turner, D. L. Cooper, D. R. Schultz, M. J. Raković, W. Fritsch, and B. Zygelman, *J. Phys. B* **34**, 2481 (2001).
- [15] J. G. Wang, A. R. Turner, D. L. Cooper, D. R. Schultz, M. J. Raković, W. Fritsch, P. C. Stancil, and B. Zygelman, *J. Phys. B* **35**, 3137 (2002).
- [16] T. E. Cravens, *Geophys. Res. Lett.* **24**, 105 (1997).
- [17] T. E. Cravens, *Astrophys. J. Lett.* **532**, L153 (2000).
- [18] D. Péquignot, S. M. V. Aldrovani, and G. Stasinska, *Astron. Astrophys.* **58**, 411 (1977); **63**, 313 (1978).
- [19] M. Kimura, J.-P. Gu, G. Hirsch, R. J. Buenker, A. Domondon, T. Watanabe, and H. Sato, *Phys. Rev. A* **56**, 1892 (1997).
- [20] R. J. Buenker, in *Current Aspects of Quantum Chemistry 1981 (Studies in Physical and Theoretical Chemistry, Vol.21)*, edited by R. Carbo (Elsevier, Amsterdam), p. 17; S. Krebs and R. J. Buenker, *J. Chem. Phys.* **103**, 5613 (1995).
- [21] B. Zygelman, D. L. Cooper, M. J. Ford, A. Dalgarno, J. Gerratt, and M. Raimondi, *Phys. Rev. A* **46**, 3846 (1992).

- [22] R. J. Buenker and S. D. Peyerimhoff, *Theor. Chim. Acta* **35**, 33 (1974); **39**, 217 (1975).
- [23] NIST Atomic Spectra Database, website <http://physics.nist.gov/asd>.
- [24] P. K. Mukherjee and K. Ohno, *Phys. Rev. A* **40**, 1753 (1989).
- [25] W. R. Gentry and C. F. Giese, *J. Chem. Phys.* **67**, 2355 (1977).
- [26] C. F. Fischer, *The Hartree-Fock Method for Atoms* (John Wiley & Sons Publication, New York, 1977).
- [27] B. H. Bransden and M. R. C. McDowell, *Charge Exchange and the Theory of Ion-Atom Collisions* (Clarendon Press, Oxford, 1992).
- [28] B. Zygelman, P. C. Stancil, N. J. Clarke, and D. L. Cooper, *Phys. Rev. A* **56**, 457 (1997).
- [29] B. R. Johnson, *J. Comput. Phys.* **13**, 445 (1973).
- [30] M. Kimura and N. F. Lane, *Adv. At. Mol. Phys.* **26**, 79 (1990).
- [31] R. K. Janev, L. P. Presnyakov, and V. P. Shevelko, *Physics of Highly Charged Ions* (New York: Springer-Verlag, 1985).
- [32] L. F. Errea, C. Harel, H. Jouin, L. Méndez, B. Pons, and A. Riera, *J. Phys. B* **27**, 3603 (1994).
- [33] M. Ritty, N. Elander, E. Brändas, and A. Barany, *J. Phys. B.* **17**, L677 (1984).
- [34] N. Shimakura and M. Kimura, *Phys. Rev. A* **44**, 1659, (1991)
- [35] S. E. Butler and A. Dalgarno, *Astro. Astrophys.* **85**, 144 (1980).
- [36] Y. H. Le Teuff, T. J. Millar and A. J. Markwick, *Astro. Astrophys. Suppl. Ser.* **146**, 157 (2000).
- [37] J. B. Kingdon and G. F. Ferland, *Astrophys. J. Suppl.* **106**, 205 (1996).
- [38] H. Shang, A. E. Glassgold, F. H. Shu, and S. Lizano, *Astrophys. J.* **564**, 853 (2002).

TABLE I: Comparison of asymptotic separated-atom energies between the MRD-CI calculations and experiments for the 18 lowest molecular states of SH^+ . These states are of symmetries $1,3,5\Sigma^-$, $1,3\Sigma^+$, $1,3\Pi$, and $1,3\Delta$.

Asymptotic atomic state	Mol. state	This work	Expt. ^a
$\text{S}^+(3s^23p^3\ ^4\text{S}^o) + \text{H}$	$1\ ^5\Sigma^-$	-3.526	-3.262
	$1\ ^3\Sigma^-$	-3.521	–
$\text{S}^+(3s^23p^3\ ^2\text{D}^o) + \text{H}$	$1\ ^1\Pi$	-1.586	-1.418
	$1\ ^1\Delta$	-1.577	–
	$1\ ^1\Sigma^-$	-1.561	–
	$1\ ^3\Pi$	-1.556	–
	$2\ ^3\Sigma^-$	-1.548	–
	$1\ ^3\Delta$	-1.544	–
	$2\ ^1\Pi$	-0.388	-0.218
$\text{S}^+(3s^23p^3\ ^2\text{P}^o) + \text{H}$	$1\ ^1\Sigma^+$	-0.366	–
	$2\ ^3\Pi$	-0.357	–
	$1\ ^3\Sigma^+$	-0.340	–
	$3\ ^3\Pi$	-0.010	0.000
$\text{S}(3s^23p^4\ ^3\text{P}) + \text{H}^+$	$3\ ^3\Sigma^-$	0.000	–
	$2\ ^1\Sigma^+$	1.180	1.121
	$3\ ^1\Pi$	1.183	–
$\text{S}(3s^23p^4\ ^1\text{D}) + \text{H}^+$	$2\ ^1\Delta$	1.189	–
	$3\ ^1\Sigma^+$	2.788	2.726
	$3\ ^1\Sigma^+$	2.788	2.726

^aRef. [23]

TABLE II: Parameters for asymptotic potentials in Eq. (4).

Asymptotic At. State	Mol. Sym.	α_d	ξ_Λ	$\langle r^2 \rangle$
$S(3s^23p^4 \ ^3P) + H^+$	Σ	18.76	-0.4	5.065
	Π	18.76	0.2	5.065
$S(3s^23p^4 \ ^1D) + H^+$	Σ	19.50	0.4	5.065
	Π	19.50	0.2	5.065
	Δ	19.50	-0.4	5.065
$S(3s^23p^4 \ ^1S) + H^+$	Σ	20.51	0	5.065
$S^+ + H(1s \ ^1S)$	Σ	4.50	0	0

TABLE III: Rate coefficients for electron capture into the $S^+(^4S^o, ^2D^o, ^2P^o) + H$ channels due to $S(^3P) + H^+$ and $S(^1D) + H^+$ collisions. *Total* represent the rate coefficients summed over the exit channels.

T	S(³ P)				S(¹ D)		
	S ⁺ (⁴ S ^o)	S ⁺ (² D ^o)	S ⁺ (² P ^o)	Total	S ⁺ (² D ^o)	S ⁺ (² P ^o)	Total
20	3.10(-16)	1.87(-15)	3.16(-13)	3.18(-13)	1.17(-16)	1.57(-18)	1.19(-16)
40	3.90(-16)	4.33(-15)	8.51(-13)	8.56(-13)	1.40(-16)	3.21(-18)	1.43(-16)
60	4.09(-16)	7.32(-15)	1.20(-12)	1.21(-12)	1.68(-16)	4.46(-18)	1.72(-16)
80	4.21(-16)	1.02(-14)	1.45(-12)	1.46(-12)	1.99(-16)	5.84(-18)	2.05(-16)
100	4.12(-16)	1.28(-14)	1.66(-12)	1.67(-12)	2.14(-16)	7.28(-18)	2.21(-16)
200	3.71(-16)	2.21(-14)	2.44(-12)	2.47(-12)	2.69(-16)	1.34(-17)	2.83(-16)
400	3.28(-16)	3.03(-14)	3.28(-12)	3.31(-12)	3.05(-16)	2.16(-17)	3.26(-16)
600	3.07(-16)	3.24(-14)	3.65(-12)	3.68(-12)	3.16(-16)	3.15(-17)	3.48(-16)
800	2.96(-16)	3.33(-14)	3.85(-12)	3.88(-12)	3.27(-16)	4.97(-17)	3.77(-16)
1000	2.93(-16)	3.43(-14)	3.98(-12)	4.01(-12)	3.42(-16)	8.39(-17)	4.26(-16)
2000	3.11(-16)	4.48(-14)	4.39(-12)	4.44(-12)	5.38(-16)	7.25(-16)	1.26(-15)
4000	4.05(-16)	1.23(-13)	5.34(-12)	5.46(-12)	1.76(-15)	6.62(-15)	8.38(-15)
6000	5.35(-16)	3.22(-13)	7.52(-12)	7.84(-12)	4.25(-15)	1.84(-14)	2.27(-14)
8000	6.97(-16)	6.64(-13)	1.11(-11)	1.18(-11)	8.78(-15)	3.56(-14)	4.44(-14)
10000	8.90(-16)	1.19(-12)	1.63(-11)	1.75(-11)	1.87(-14)	6.83(-14)	8.70(-14)
20000	8.10(-15)	8.65(-12)	6.92(-11)	7.79(-11)	4.45(-13)	1.64(-12)	2.09(-12)
40000	7.94(-13)	5.95(-11)	3.13(-10)	3.74(-10)	7.64(-12)	1.63(-11)	2.39(-11)
60000	4.34(-12)	1.52(-10)	6.97(-10)	8.53(-10)	2.68(-11)	3.54(-11)	6.23(-11)
80000	1.03(-11)	2.69(-10)	1.17(-09)	1.45(-09)	5.51(-11)	5.25(-11)	1.08(-10)
100000	1.77(-11)	4.02(-10)	1.68(-09)	2.10(-09)	8.83(-11)	6.76(-11)	1.56(-10)
200000	6.30(-11)	1.13(-09)	4.40(-09)	5.59(-09)	2.65(-10)	1.52(-10)	4.17(-10)
400000	1.59(-10)	2.53(-09)	9.34(-09)	1.20(-08)	6.16(-10)	5.35(-10)	1.15(-09)
600000	2.48(-10)	3.76(-09)	1.35(-08)	1.75(-08)	1.04(-09)	1.24(-09)	2.28(-09)
800000	3.40(-10)	4.83(-09)	1.70(-08)	2.22(-08)	1.56(-09)	2.17(-09)	3.73(-09)
1000000	4.39(-10)	5.81(-09)	2.01(-08)	2.64(-08)	2.19(-09)	3.21(-09)	5.40(-09)

$${}^a A(-B) = A \times 10^{-B}$$

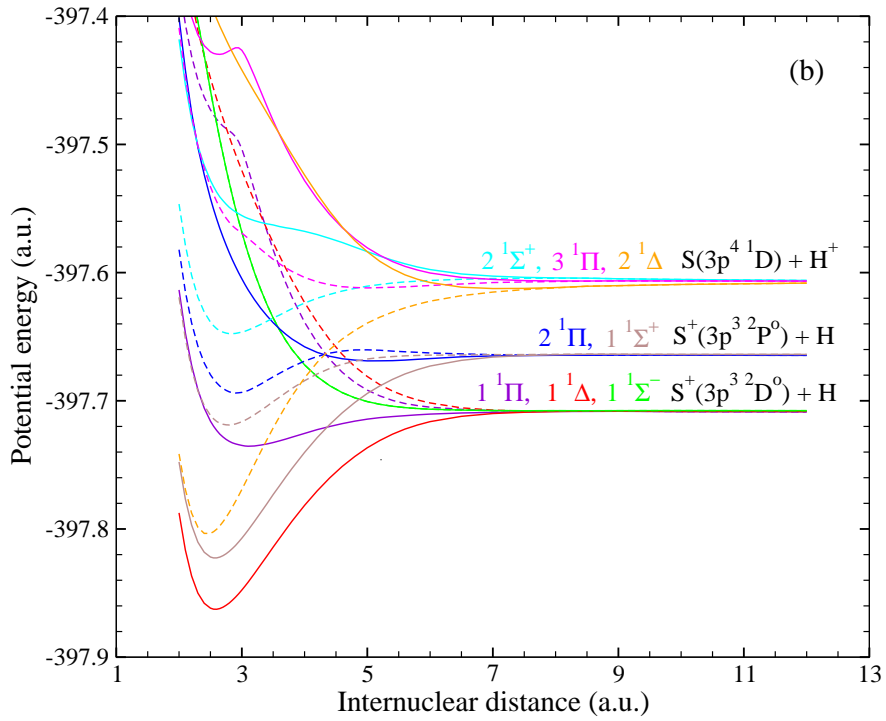
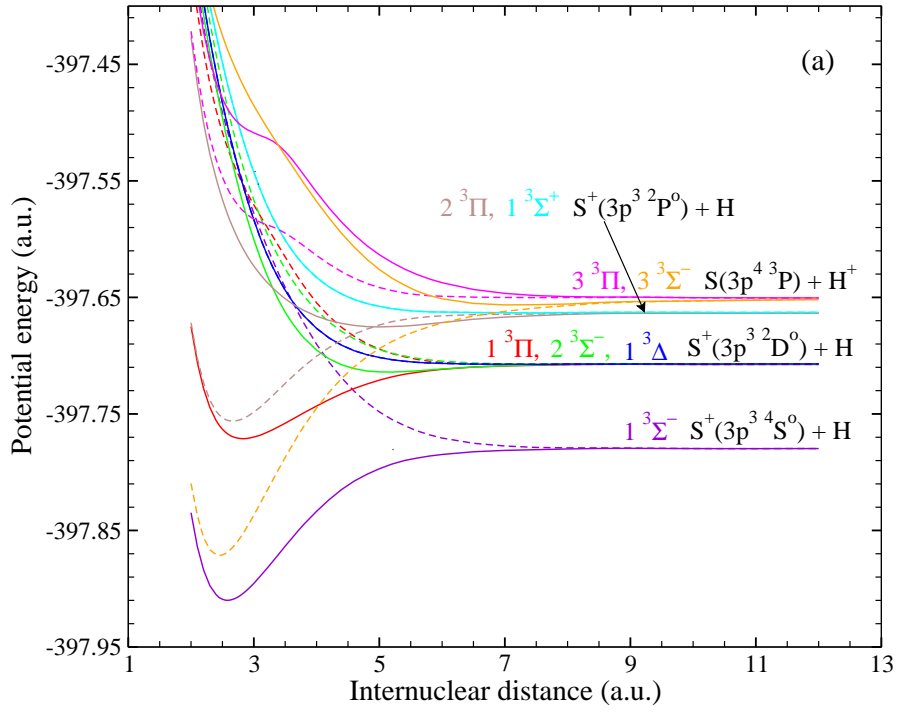


FIG. 1: The adiabatic (—) and diagonal diabatic (----) potential energies for the triplet (a) and singlet (b) states of the SH^+ system as a function of internuclear distance R .

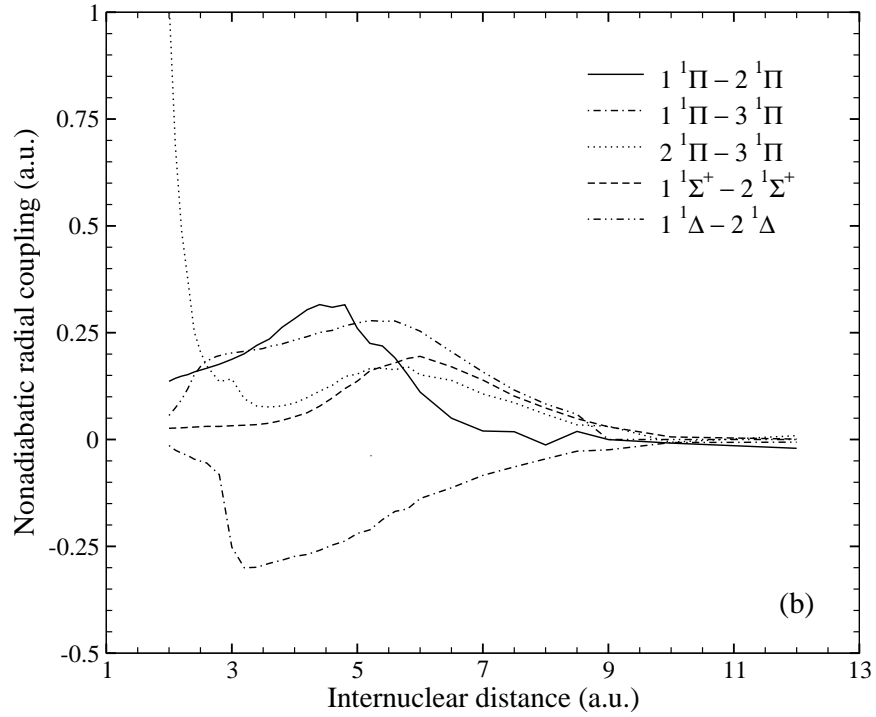
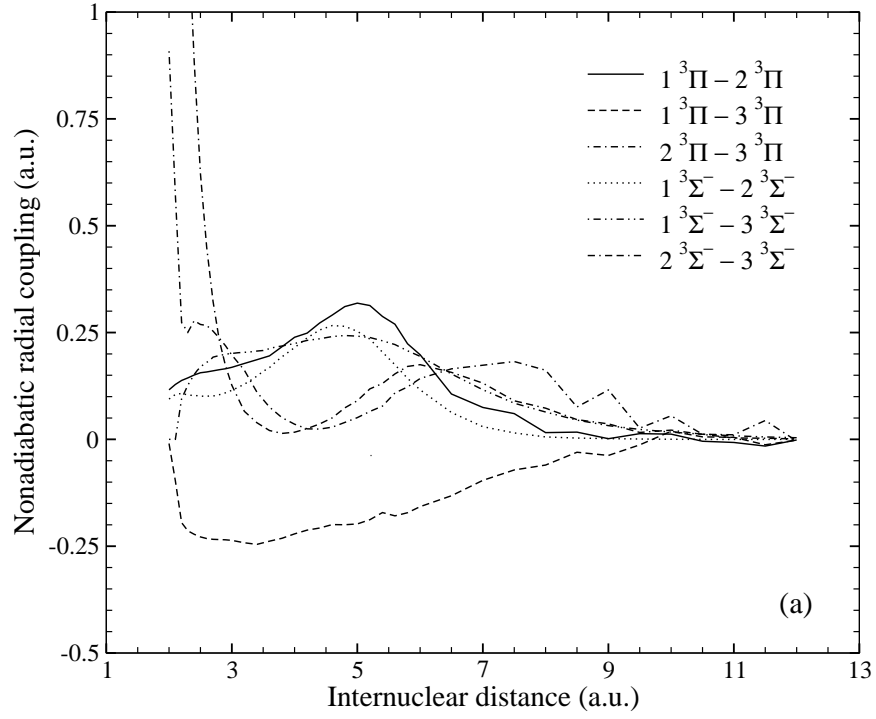


FIG. 2: The (a) ${}^3\Pi$ and ${}^3\Sigma^-$ and (b) ${}^1\Pi$, ${}^1\Sigma^+$, and ${}^1\Delta$ nonadiabatic radial couplings for the SH^+ system as a function of internuclear distance R .

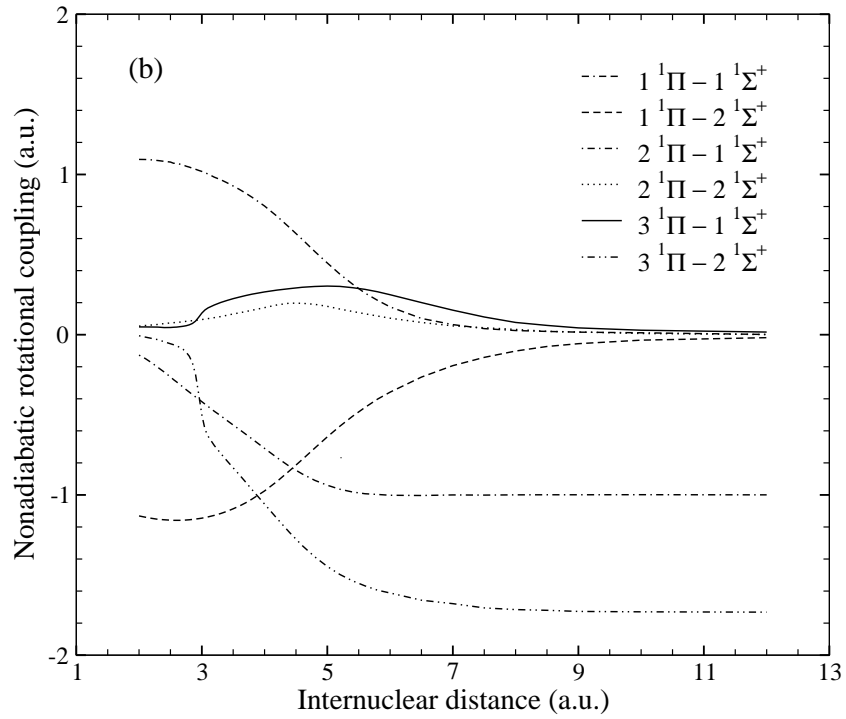
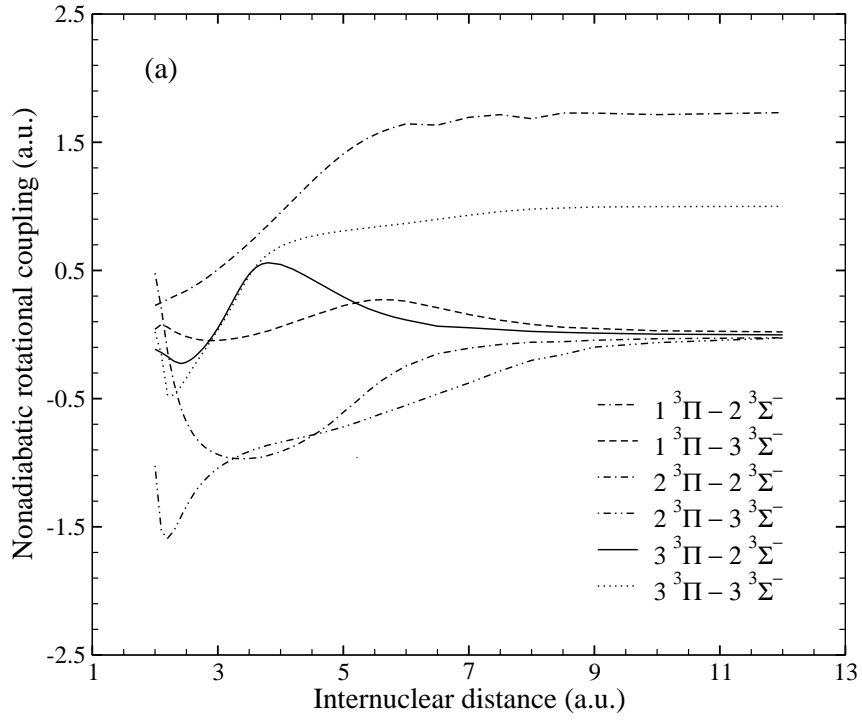


FIG. 3: The representative nonadiabatic rotational couplings (a) between the triplet $^3\Pi$ and $^3\Sigma^-$ states and (b) between the singlet $^1\Pi$ and $^1\Sigma^+$ states of the SH^+ system as a function of internuclear distance R .

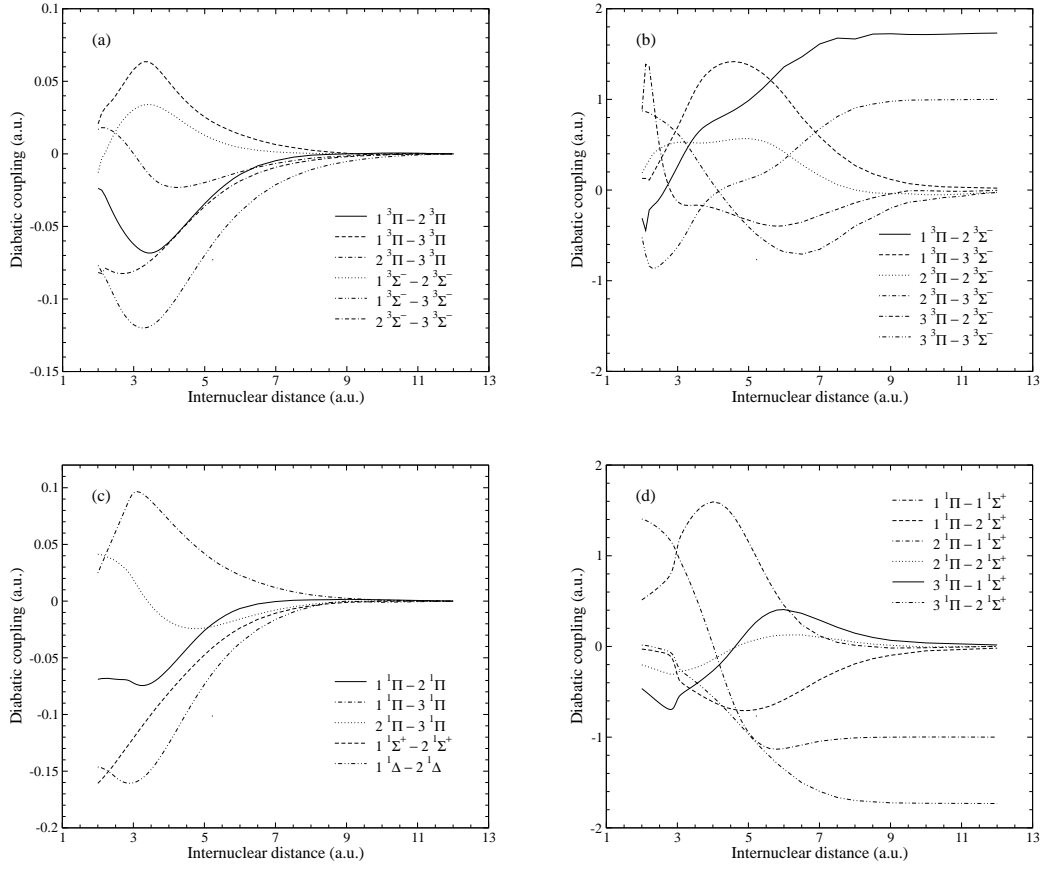


FIG. 4: The representative off-diagonal diabatic potentials for the triplet (a), (b) and singlet (c), (d) states of SH^+ system as a function of internuclear distance R .

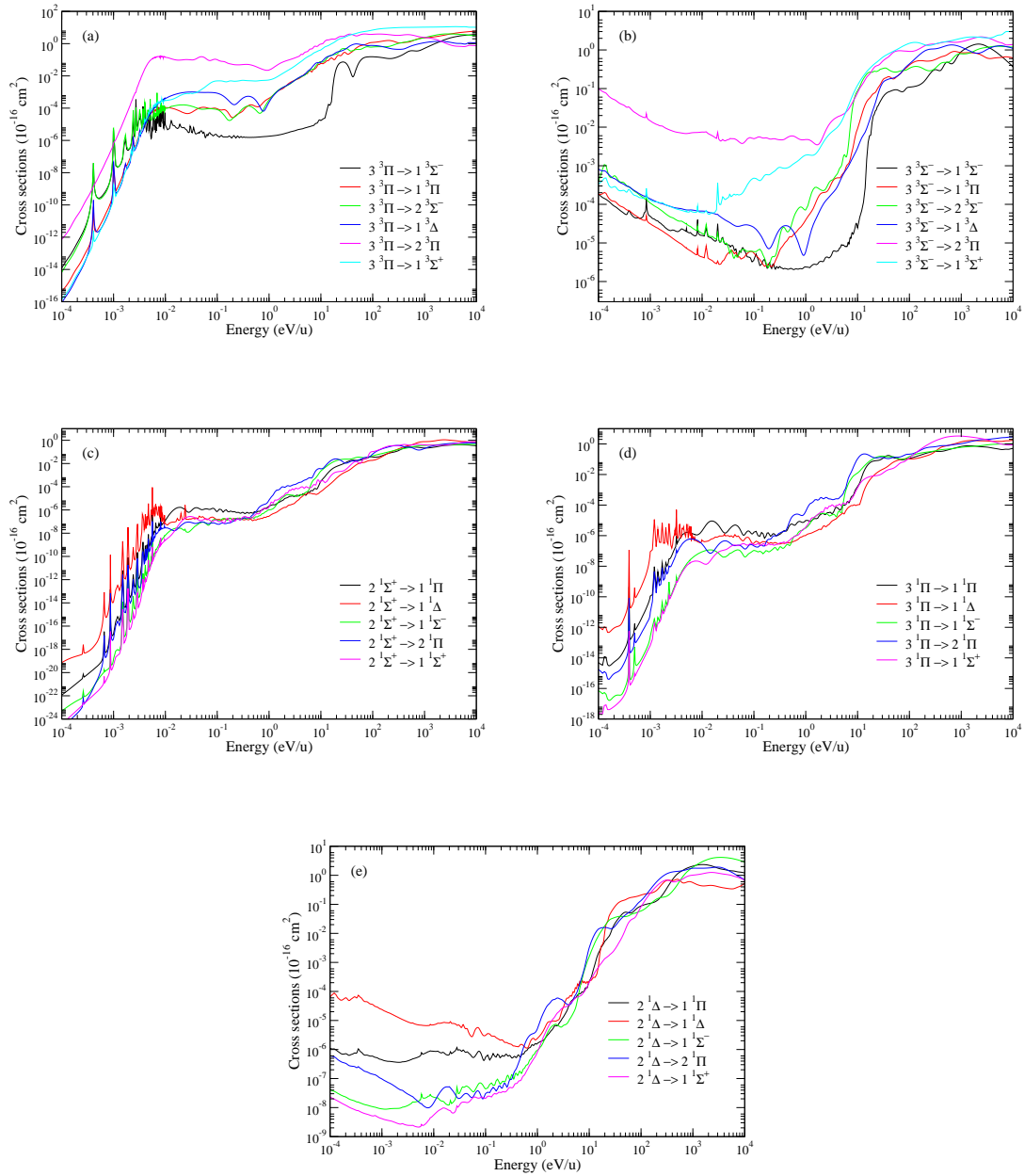


FIG. 5: State-to-state charge-transfer cross sections for the SH^+ system as a function of relative collision energy E . (a) and (b) represent transitions between the triplet states; and (c), (d), and (e) are transitions between the singlet states.

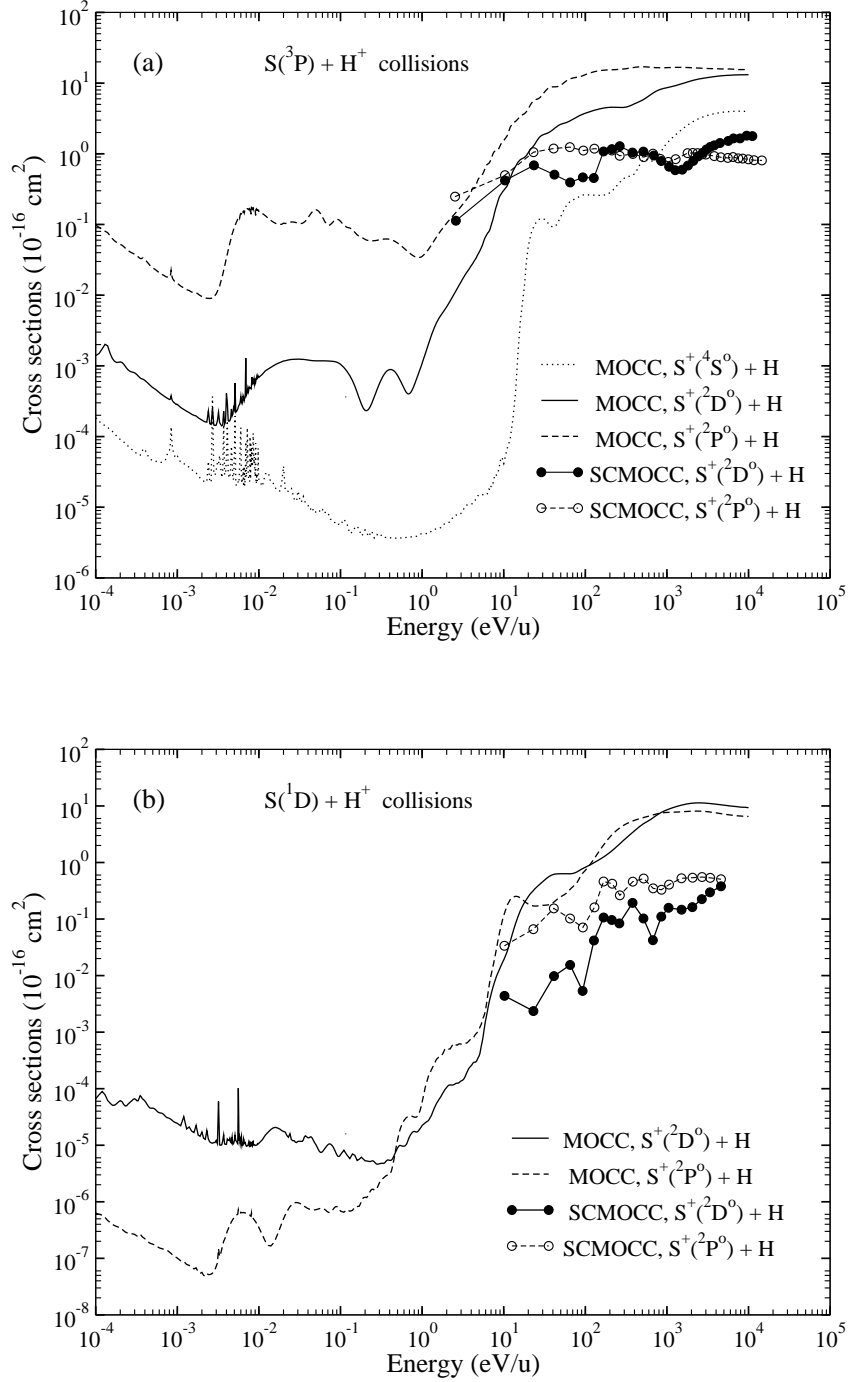


FIG. 6: Comparison of state-selective charge-transfer cross sections obtained with the present QMOCC method and those with the SMOCC method (Ref. [19]). (a) represents charge transfer into $S^+(^4S^0, ^2D^0, ^2P^0) + H$ due to $S(^3P) + H^+$ collisions, and (b) corresponds to charge transfer into $S^+(^2D^0, ^2P^0) + H$ due to $S(^1D) + H^+$ collisions.

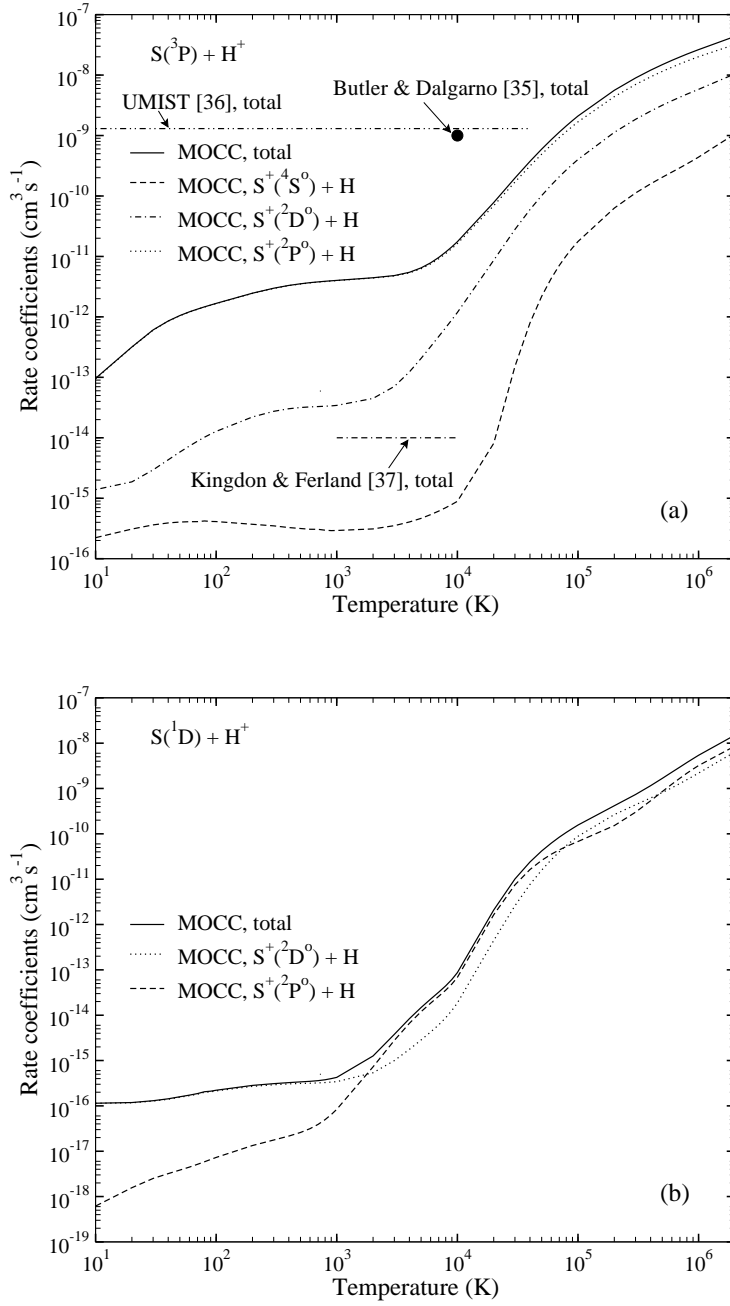


FIG. 7: Rate coefficients for charge transfer into $\text{S}^+(^4\text{S}^o, ^2\text{D}^o, ^2\text{P}^o) + \text{H}$ for collisions of (a) ground-state $\text{S}(^3\text{P})$ with H^+ and of (b) excited-state $\text{S}(^1\text{D})$ with H^+ as a function of temperature T .